DOI: 10.1002/ejic.201100218

Synthesis, Structure, and Behavior in Solution of the Dawson Thio Derivative $[(P_2W_{17}O_{61})_2(H_4Mo_4S_4O_6)]^{16-}$

Marie-Anne Pilette,[a] Sébastien Floquet,[a] Jérôme Marrot,[a] and Emmanuel Cadot*[a]

Keywords: Molybdenum / Tungsten / Polyoxometalates / Sulfur / Isomerization

The $[(P_4W_{34}O_{61})_2\{Mo_4S_4O_4(OH_2)_2\}]^{16-}$ anion was obtained by the stereospecific addition of the $[Mo_2S_2O_2]^{2+}$ oxothio cation to the monovacant α_2-$[P_2W_{17}O_{61}]^{10-}$ anion. The mixed salt $K_9Na_7[(P_2W_{17}O_{61})_2\{Mo_4S_4O_4(OH_2)_2\}]\cdot 50H_2O$ was isolated as single crystals and characterized by X-ray diffraction. The analysis reveals that the anion adopts a "sandwich-like" dimeric structure in which the two α_2-$[P_2W_{17}O_{61}]^{10-}$ subunits are assembled in a *transoid* disposition with respect to the central cluster $\{H_4Mo_4S_4O_6\}$. In aqueous solution, an isomerization process is evidenced by ^{31}P NMR spectroscopy and interpreted as the formation of the related *cisoid* isomer. A ratio of 30:70 of the *transoid* and *cisoid* isomers was found at equilibrium. The kinetic constants and activation parameters of the isomerization process were determined by variable-temperature ^{31}P NMR experiments. At 303 K, the process was slow ($t_{1/2}$ = 160 min). The activation parameters are discussed with regard to a possible isomerization mechanism.

Introduction

Current research activity into the chemistry of polyoxometalates (POMs) is largely driven by potential applications in catalysis,[1–3] medicine,[4,5] magnetism,[6–9] materials sciences,[10,11] and nanotechnology,[12] which require a continuous improvement of efficient and adapted functional molecular materials. POM compounds, often described as soluble, discrete metal oxide frameworks, can be finely tuned at the molecular level. The chemistry of metal sulfur clusters has been investigated for a long time, especially for their ability to mimic the active sites of several metalloenzymes.[13,14] For instance, some nitrogenase enzymes have been found to contain $\{Fe_4S_4\}$-based clusters as the active site with a Mo–Fe cofactor associate.[15] The effect of sulfur donor ligands on the chemistry of molybdenum is therefore of significant interest.[16] Mainly driven by hydrodesulfurization (HDS) industrial processes, some important iron-free systems such as molybdenum sulfide dimers and their cationic derivatives used as models for MoS_2-based surfaces have been shown to constitute efficient electrocatalysts for hydrogen production.[17–19] In this field, we recently demonstrated that cyclic molecular architectures obtained from the condensation of the aqua ion $[Mo_2O_2S_2(OH_2)_6]^{2+}$ induce a catalytic functionality for the reduction of protons into hydrogen in either organic or aqueous media.[20,21] From this result, one of the basic ideas for the design of robust, inexpensive, and efficient electrocatalytic materials involves combining the $\{Mo_2O_2S_2\}$ binuclear fragment with an electroactive polyoxometalate. Based on the fact that sulfur(II) ions are generally invoked for stabilizing the lower oxidation states (+V, +IV, and +III) of Mo or W atoms,[22] the incorporation of S–Mo(W) clusters into the POM framework is expected to modify its electronic properties. A fruitful approach to the synthesis of sulfur-containing polyoxometalates has been developed that involves treating the electrophilic core $\{Mo_2O_2S_2\}^{2+}$ with vacant polyoxotungstate ions.[23–27] With regard to the potential of the method and the growth of interest in such compounds, this field of investigation continues to be one of our main focuses. We present herein the synthesis and characterization in the solid state and solution of the oxothio heteropolyanion obtained from the direct addition of the dication $\{Mo_2O_2S_2\}^{2+}$ to the monovacant polyanion α_2-$[P_2W_{17}O_{61}]^{10-}$.

Results and Discussion

Molecular Structure of $[(P_2W_{17}O_{61})_2\{Mo_4S_4O_4(OH_2)_2\}]^{16-}$ (1)

The molecular representation of the structure of **1** (Figure 1) reveals a dimeric association of two α_2-$[P_2W_{17}O_{61}]^{10-}$ subunits sandwiching two $\{Mo_2O_2S_2\}$ oxothio fragments. Each Mo atom is symmetrically bonded to two oxygen atoms delimiting the vacancy within the α_2-$[P_2W_{17}O_{61}]^{10-}$ subunit. In this arrangement, the POM subunits act as bisbidentate ligands, constraining the two $\{Mo_2O_2S_2\}$ moieties to interact through a quasi-linear double Mo–O–Mo bridge. In the resulting compound, the two α_2-

[a] Institut de Lavoisier de Versailles, UMR CNRS 8180, Université de Versailles,
45 Avenue des Etats-Unis, 78035 Versailles, France
Fax: +33-1-39-25-43-81
E-mail: cadot@chimie.uvsq.fr

Supporting information for this article is available on the WWW under http://dx.doi.org/10.1002/ejic.201100218.

$[P_2W_{17}O_{61}]^{10-}$ subunits are equivalent and display a 180° staggered arrangement (Figure 1). According to the terminology proposed by Termes and Pope for uranyl-containing complexes,[28] the anion **1** is a *transoid* isomer. The two Mo atoms of the asymmetric unit are symmetrically placed over, rather than in, the vacancy site in each α_2-$[P_2W_{17}O_{61}]^{10-}$. A similar situation has previously been reported by Finke and co-workers for the structure of the "$\{P_2W_{17}Ru\}_2$–O" dimer.[29] In the latter, the two monovacant heteropolyanions α_2-$[P_2W_{17}O_{61}]^{10-}$ are connected to a central $[Cl–Ru–O–Ru–Cl]^{4+}$ cluster (instead of $\{H_4Mo_4S_4O_6\}^{4+}$) in a *transoid* fashion. The *cisoid* disposition has also been observed. For example, in the sandwich-like compound "$[(P_2W_{17}O_{61})_2\{Mo_3S_4(OH_2)_3(OH)\}_2]^{14-}$", the two POM subunits are anchored to the central dimeric cationic $\{Mo_3S_4(OH)_2Mo_3S_4\}^{6+}$ cluster in an "eclipsed" fashion to give the *cisoid* isomer.[30] However, the structure of **1** reveals a slight disorder that consists of the equal distribution of the Mo1 atom over two positions, labeled A and B (see Figure S1 in the Supporting Information). Such disorder induces some ambiguity for the complete description of the structure because two distinct distances are generated for the terminal Mo–O bonds. The long Mo1B–O distance [2.16(15) Å] reflects the presence of a terminal aqua ligand, whereas the shortest Mo1A–O distance [1.73(15) Å] is characteristic of a terminal oxo group. The presence of either an oxo group or aqua ligand attached to Mo1A or Mo1B, respectively, fully confirms the bond valence sum (BVS) calculations[31,32] (for an unprotonated oxygen atom, the BVS values fall between –2.2 and –1.8, whereas the diprotonated O41 and O42 have values of –0.41 and –0.48, respectively). A similar disordered distribution was found in the closely related compound $[(PW_{11}O_{39})_2(H_4Mo_4S_4O_6)]^{10-}$, leading to two possible arrangements for the central cluster.[24] Because the stereochemistries of both Keggin and Dawson monovacant anions are known to be similar, the structural disorder in **1** should be solved in the same way. One possibility is a *syn* isomer in which the two water molecules are attached to two nearby Mo atoms belonging to the same dimer (C_2 symmetry), and the other is the *anti* isomer with two water molecules each linked to two separate Mo atoms related by an inversion center (C_i symmetry). Both arrangements are depicted in Figure 2. DFT calculations were carried out on both conformations. Unfortunately, these did not permit the two isomers to be discriminated energetically. The μ-disulfido-bridged dinuclear molybdenum(V) moiety has been observed for both *syn* and *anti* stereochemistries,[33,34] and in the present case, the geometrical data, bond lengths, and angles are compatible with both geometries. The bonding schemes in the *syn* and *anti* isomers of the $[Mo_2S_4]^{2+}$ core were studied theoretically and calculations using the extended Hückel and Fenske–Hall approaches indicated that the *syn* isomer is the most stable.[35] Note that the *anti* isomer has been exclusively obtained in anhydrous solvent as CH_3CN.[34] In this case, the starting material used was the $[Mo_2O_2S_9]^{2-}$ anion, which permits free rotation of the two Mo=O moieties along the Mo–S–Mo bridges, producing in CH_3CN solution the two *syn* and *anti* isomers.[36] The conversion of the *anti* into the *syn* conformation is H_3O^+-catalyzed and thus the presence of the *anti* conformation in water containing solvent is likely not expected.[34] These features rather argue for a *syn–syn* interaction, depicted in Figure 2a, without any change in the original *syn* conformation of the dinuclear precursor through the assembling process.

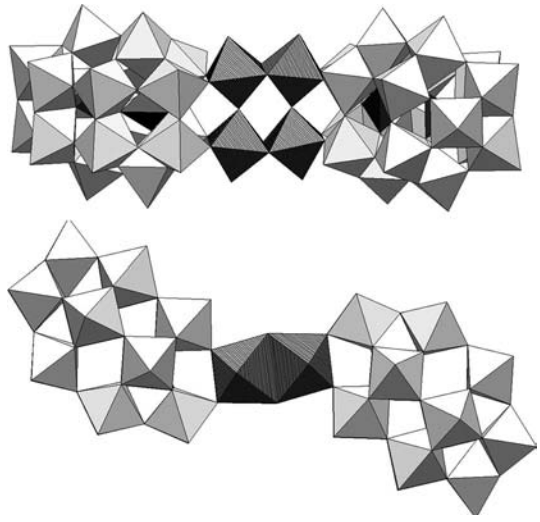

Figure 1. Polyhedron perspective views of the *transoid* anion $[(P_2W_{17}O_{61})_2\{Mo_4S_4O_4(OH_2)_2\}]^{16-}$. The central cluster $\{H_4Mo_4S_4O_6\}$ is represented by dark-grey polyhedra.

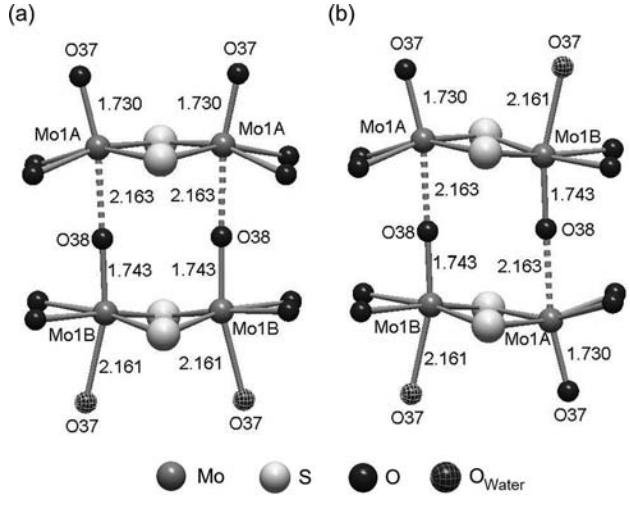

Figure 2. Ball-and-stick labeled models of the two possible arrangements of the central cluster $\{H_4Mo_4S_4O_6\}$. (a) *syn–syn* conformation of the $\{H_4Mo_4S_4O_6\}$ central core; (b) *anti–anti* conformation of the $\{H_4Mo_4S_4O_6\}$ central core.

^{31}P NMR in Solution

The ^{31}P NMR spectrum of the *transoid*-$[(P_2W_{17}O_{61})_2\{Mo_4S_4O_4(OH_2)_2\}]^{16-}$ is given in Figure 3a. It consists of two single lines located at –7.53 and –13.38 ppm with 1:1 integration evidencing that (i) the $\{P_2W_{17}\}$ subunits are coordinated to $\{Mo_2O_2S_2\}$ fragments (the ^{31}P NMR of the

$\{P_2W_{17}\}$ monovacant POM gives two lines at –7.10 and –13.60 ppm under the same experimental conditions) and (ii) the two $\{P_2W_{17}\}$ subunits of the dimer are equivalent, in agreement with the single-crystal X-ray diffraction study. In accord with the report on the dimer $[(PW_{11}O_{39})_2(H_4Mo_4S_4O_6)]^{10-}$,[24] the ^{31}P NMR spectrum of **1** is time-dependent and two additional lines at –7.31 and –13.32 ppm gradually grow in intensity to reach a constant value characteristic of the equilibrium state (see Figure 3b). Taking into account the large distance between the two $\{P_2W_{17}\}$ polyanions, which prevents any mutual steric influence and the lability of the Mo–O bonds involved in the Mo–O–W junctions, which has been established in previous studies,[23–25,37] the very similar ^{31}P NMR features argue for an isomeric system. The *transoid* arrangement, which has been structurally characterized by single-crystal X-ray crystallography, can give the *cisoid* isomer simply by the rotation of one $\{P_2W_{17}\}$ subunit through 180° with respect to the other, as depicted in Scheme 1, in agreement with the previous study of the dimeric compound $[(PW_{11}O_{39})_2(H_4Mo_4S_4O_6)]^{10-}$.[24] In the *transoid* and *cisoid* compounds, the two "eclipsed" $\{P_2W_{17}\}$ subunits exhibit the same mode of connection within the central tetranuclear core and thus appear equivalent in both isomers. The two additional signals at –7.31 and –13.32 ppm are then assigned to the *cisoid* isomer of the $[(P_2W_{17}O_{61})_2\{Mo_4S_4O_4(OH_2)_2\}]^{16-}$ compound. The former signal at –7.31 ppm is attributed to the phosphate group close to the vacancy site and the coordinated $\{Mo_2O_2S_2\}$ moieties, whereas the signal at –13.32 ppm, less affected by the isomerization process (–13.38 ppm for the *transoid* isomer), corresponds to the opposite phosphate, encapsulated within the $\{PW_9O_{34}\}$ moiety. The kinetics of the isomerization process was studied in the temperature range 293–323 K. The fractions of *cisoid* isomer versus time are graphically shown in Figure 4. A simple kinetic model for the isomerization of the *cisoid* and *transoid* arrangements [equilibrium (1)] is described by the rate constants k_1 and k_{-1} and the equilibrium constant $K = [cisoid]/[transoid]$.

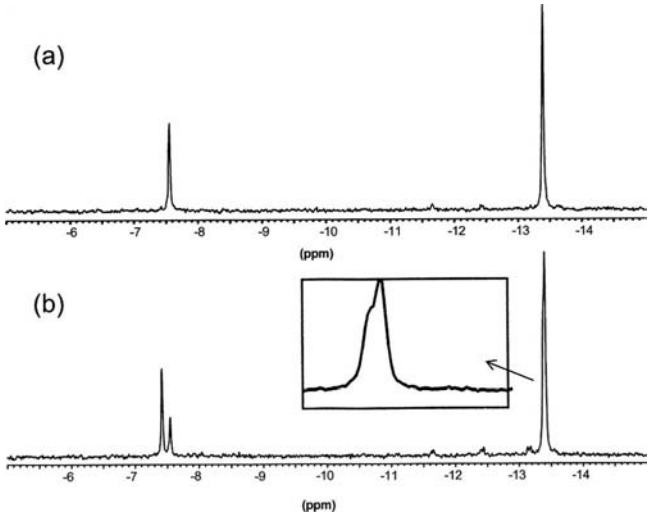

Figure 3. ^{31}P NMR spectra of (a) pure *transoid*-$[(P_2W_{17}O_{61})_2\{Mo_4S_4O_4(OH_2)_2\}]^{16-}$ in D_2O and (b) a mixture of *transoid*-$[(P_2W_{17}O_{61})_2\{Mo_4S_4O_4(OH_2)_2\}]^{16-}$ and *cisoid*-$[(P_2W_{17}O_{61})_2\{Mo_4S_4O_4(OH_2)_2\}]^{16-}$ isomers in D_2O at equilibrium.

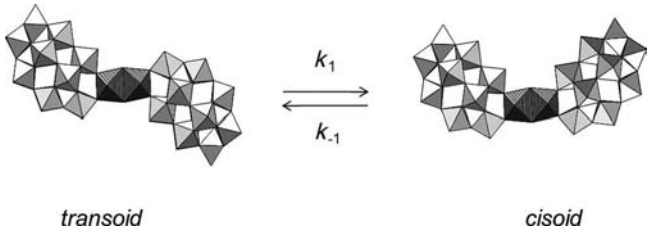

Scheme 1. Schematic representation of the isomerization process.

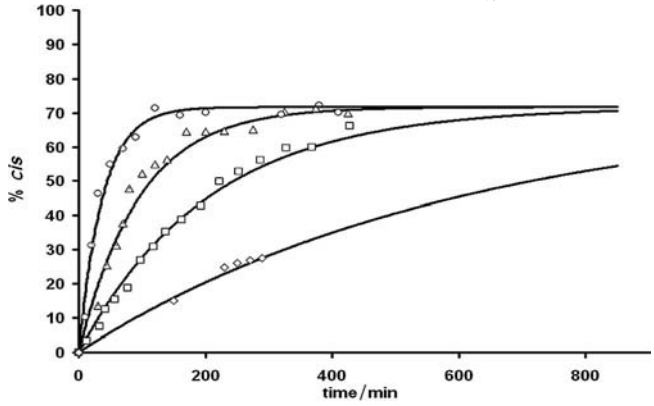

Figure 4. Kinetic plots for the isomerization of the *transoid*-$[(P_2W_{17}O_{61})_2\{Mo_4S_4O_4(OH_2)_2\}]^{16-}$ and the *cisoid*-$[(P_2W_{17}O_{61})_2\{Mo_4S_4O_4(OH_2)_2\}]^{16-}$ isomers at 293 (◇), 303 (□), 313 (Δ), and 323 K (○). Dotted lines correspond to the calculated values determined from Equation (2) and from the data in Table 1.

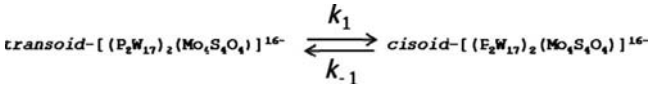

(1)

Supposing a first-order process for equilibrium (1), the rate constants k_1 can be determined for each temperature by taking into account the initial rates. The rate constants k_{-1} are deduced from k_1 and K by using the expression $K = k_1/k_{-1}$, with K remaining nearly constant in the 293–323 K range (see Table 1). The proportions of the *cisoid* isomer with time can be calculated by introducing the values of these parameters into Equation (2), deduced from equilibrium (1).

$$\%(cisoid) = 100 \times [k_1/(k_1 + k_{-1})] \times \exp[-(k_1 + k_{-1})t] \quad (2)$$

Table 1. Kinetic parameters of equilibrium (1).

T [K]	k_1 [min^{-1}]	k_{-1} [min^{-1}]	K
293	0.12	0.047	2.54
303	0.35	0.137	2.54
313	0.75	0.295	2.54
323	1.90	0.748	2.54

As depicted in the full lines in Figure 4, the calculated values for the proportion of the *cisoid* as a function of time at various temperatures are in good agreement with the experimental data, thus supporting the proposed kinetic model. Finally, starting from the values of k_1 and k_{-1}, the activation energy of the isomerization process can be determined from an Arrhenius plot (Figure S2, Supporting Information), derived from Equations (3) and (3′).

$$k_i = A \times \exp[\{-E_a(i)\}/\{RT\}] \quad (3)$$

$$\ln(k_i) = [\{-E_a(i)\}/\{RT\}] + \ln(A) \quad (3')$$

Equation (3′) gives two lines from which the activation energies for the isomerization of the two isomers $E_a(1)$ and $E_a(-1)$ are both found to be 71.2 kJ mol^{-1}. The Eyring plots for the isomerization processes are given in Figure 5 and the values of $\Delta G^{\neq}$, $\Delta H^{\neq}$, and $\Delta S^{\neq}$ are listed in Table 2. These data reveal that the activation enthalpy is equal for both reactions [$\Delta H^{\neq}(1) = \Delta H^{\neq}(-1) = 68.6$ kJ mol^{-1}] and that the main difference is observed for the activation entropy [$\Delta S^{\neq}(1) = -27.7$ J K^{-1} mol^{-1}, $\Delta S^{\neq}(-1) = -35.5$ J K^{-1} mol^{-1}]. These results show that the kinetic stability of the isomers is mainly entropic in origin, a probable consequence of the nature of the activated species issuing from either the *transoid* or *cisoid* isomer. Note that the $\Delta H^{\neq}$ value determined in this study is significantly lower than the activation energy determined by Anderson and Hill[38] for the isomerization of β to α of the Dawson polyanion $[P_2W_{18}O_{61}]^{6-}$ ($\Delta H^{\neq} = 83$ kJ mol^{-1}), which corresponds formally to the rotation of a trimetallic tungstate group $[W_3O_{13}]$ through a concerted mechanism involving the breaking and re-formation of six W–O bonds. In the β → α isomerization process, the determining step was identified as the OH^- hydrolytic attack, breaking a W–O–W corner junction to give a pseudo-lacunary intermediate. The lower value of $\Delta H^{\neq} = 68.6$ kJ mol^{-1} observed in our study could be related to the weakness of the Mo–O bond within Mo–O–W bridge compared with the W–O–W junctions in the Dawson polyanion $[P_2W_{18}O_{61}]^{6-}$. From a thermodynamic point of view, the nondependent behavior of the equilibrium constant K on temperature is consistent with a standard enthalpy close to zero ($\Delta_r H° \approx 0$), which means that the isomerization process is mainly entropy-driven. The thermodynamic parameters $\Delta_r G°$, $\Delta_r H°$, and $\Delta_r S°$ at T = 293 K are given in Table 2.

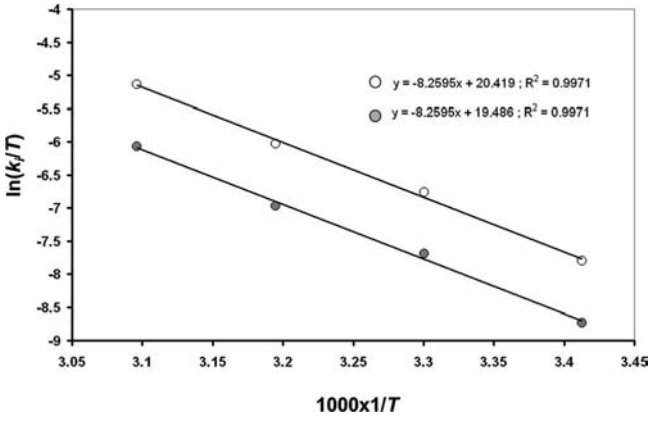

Figure 5. Temperature dependence of the isomerization process (Eyring plot). (○) Reaction (1) (*transoid* → *cisoid*); (●) reaction (–1) (*cisoid* → *transoid*).

Table 2. Activation and thermodynamic parameters at 293 K for equilibrium (1).

	Activation parameters		
	$\Delta H^{\neq}$ [kJ mol^{-1}]	$\Delta S^{\neq}$ [J K^{-1} mol^{-1}]	$\Delta G^{\neq}$ [kJ mol^{-1}]
Reaction (1)	68.6	–27.7	76.7
Reaction (–1)	68.6	–35.5	79.0
	Thermodynamic parameters		
	$\Delta_r H°$ [kJ mol^{-1}]	$\Delta_r S°$ [J K^{-1} mol^{-1}]	$\Delta_r G°$ [kJ mol^{-1}]
	≈ 0	7.75	–2.27

UV/Vis Studies in Solution

The batch spectrophotometric titration of a solution of $\{Mo_2O_2S_2\}^{2+}$ by $\{P_2W_{17}\}$ was performed in aqueous medium using a constant concentration of oxothio cation $\{Mo_2O_2S_2\}^{2+}$ (1.74×10^{-3} M) and variable amounts of $\{P_2W_{17}\}$ in aqueous solution to obtain ratios of $\{P_2W_{17}\}/\{Mo_2O_2S_2\}^{2+}$ in the range 0 to 3.4. The resulting electronic spectra were recorded in quartz cells between 250 and 750 nm and are presented in Figure 6a. By mixing the two components, the solution rapidly turns red-brown. Absorptions in the 400–500 nm range are characteristic of the red-brown thio derivatives of POMs,[24–27,37] as the used precursors $\{Mo_2O_2S_2(OH_2)_6\}^{2+}$ and $\{P_2W_{17}\}$ do not exhibit significant absorptions in this region. The gradual addition of $\{P_2W_{17}\}$ to a constant quantity of $\{Mo_2O_2S_2\}^{2+}$ translates

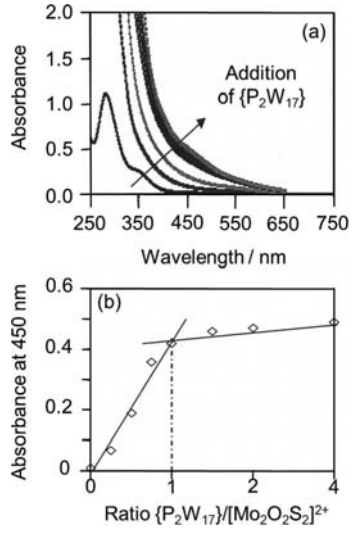

Figure 6. (a) Spectroscopic titration of $[Mo_2O_2S_2]^{2+}$ against $[P_2W_{17}O_{61}]^{10-}$ in aqueous solution. (b) Variation of the absorbance measured at 450 nm as a function of the ratio $[P_2W_{17}O_{61}]^{10-}/[Mo_2O_2S_2]^{2+}$.

into an increase in the absorbance in this region (see Figure 6a). In particular, the variation of the absorbance at 450 nm as a function of the ratio $\{P_2W_{17}\}/\{Mo_2O_2S_2\}^{2+}$ (Figure 6b) displays two linear portions with a break point at a ratio $\{P_2W_{17}\}/\{Mo_2O_2S_2\}^{2+}$ of 1, which confirms the stoichiometry of the complex $[(P_2W_{17}O_{61})_2\{Mo_4S_4O_4(OH_2)_2\}]^{16-}$ and the quantitative formation of Dawson thio derivatives, distributed as *cisoid* and *transoid* isomers.

Conclusion

The reaction of the monovacant α_2-$[P_2W_{17}O_{61}]^{10-}$ anion with the acidic oxothio cation $[Mo_2O_2S_2]^{2+}$ leads to a new "sandwich-like" compound, enclosing an unusual central cluster $\{H_4Mo_4S_4O_6\}$. Although a *transoid* arrangement is characterized in the solid state, an isomerization process between *cisoid* and *transoid* isomers was evidenced by ^{31}P NMR spectroscopy and the kinetics of this process were studied by variable-temperature NMR spectroscopy. This process highlights the high versatility of the association between POMs and the $[Mo_2O_2S_2]^{2+}$ fragment and prompts us to develop further this kind of association to produce original dynamic supramolecular compounds.

Experimental Section

Physical Methods: Water content was determined by thermal gravimetric analysis (tga7, Perkin–Elmer). Infrared spectra were recorded with a Magna 550 Nicolet spectrophotometer using KBr pellets. Elemental analysis was performed by the Service Central d'Analyses du CNRS. ^{31}P NMR spectra were recorded for solutions of 10^{-2}–10^{-1} mol L^{-1} of the polyanion with a Bruker Avance-300 spectrometer operating at a nominal frequency of 121.5 MHz. Spectra were referenced to external 85% H_3PO_4 in 5 mm tubes. For the kinetic study, ^{31}P NMR samples were prepared by dissolving 0.35 g of **2** in 500 μL of 1.6 mol L^{-1} $NaClO_4$ in H_2O/D_2O at 0 °C. The solutions were then concentrated to allow acquisitions of each spectrum within 2 min (240 scans) at temperatures ranging between T = 293 and 323 K. UV/Vis spectra were recorded at room temperature with a Perkin–Elmer Lambda 19 spectrophotometer using 0.1 cm quartz cells.

X-ray Crystallography: A well-shaped red-brown crystal ($0.04 \times 0.02 \times 0.02$ mm^3) of $K_9Na_7[(P_2W_{17}O_{61})_2\{Mo_4S_4O_4(OH_2)_2\}]\cdot 50H_2O$ was mounted in a Lindemann tube for indexing and intensity data collection at room temperature using a Smart CCD diffractometer with graphite-monochromated Mo-K_α radiation (λ = 0.71073 Å) at room temperature. Unit cell dimensions were refined by a least-squares fit of reflections. Of the 31381 reflections, 6463 unique reflections (R_{int} = 0.1412) and 9695 were considered [$I > 2\sigma(I)$]. Corrections for polarization and Lorentzian effects were applied. An absorption correction was performed by using the SADABS program[39] based on the methods of Blessing.[40] Direct methods were used to locate the heaviest atoms and then sulfur, potassium, phosphorus, and oxygen atoms were found from successive refinements by full-matrix least-squares methods using the SHELX-TL package.[41,42] The final refinement cycle, including the atomic coordinates, anisotropic thermal parameters (atoms of the heteropolyanion), and isotropic thermal parameters (for the K^+/Na^+ cations and oxygen atoms of crystallization water molecules) converged towards R_1 = 0.0573 and wR_2 = 0.1264. Crystallographic data are given in Table 3. Note that some water molecules and sodium and potassium cations were found disordered, whereas the molybdenum atoms of the central $[Mo_4S_4O_4(OH_2)_2]$ cluster were found statistically distributed over two positions (SOF = 0.5). Further details on the crystal structure investigation may be obtained from the Fachinformationszentrum Karlsruhe , 76344 Eggenstein-Leopoldshafen, Germany (fax: +49-7247-808-666; e-mail: crysdata@fiz-karlsruhe.de), on quoting the depository number CSD-422723.

Table 3. Crystallographic data for $K_9Na_7[(P_2W_{17}O_{61})_2\{Mo_4S_4O_4(OH_2)_2\}]\cdot 50H_2O$.

Formula	$H_{104}K_9Mo_4Na_7O_{178}P_4S_4W_{34}$
M_r	10351.8
Color	brown
Crystal dimensions [mm^3]	$0.04 \times 0.02 \times 0.02$
Crystal system	orthorhombic
Space group	I_{bam}
T [K]	296(2)
a [Å]	38.0443(4)
b [Å]	20.6186(3)
c [Å]	21.8730(3)
V [Å^3]	17157.6(4)
Z	4
$\rho_{calcd.}$ [g cm^{-3}]	4.014
μ [mm^{-1}]	23.435
θ range [°]	1.07–23.53
Reflections measured	31381
Unique reflections (R_{int})	6463 (0.1412)
Observed [$I > 2\sigma(I)$]	9695
Refined parameters	563
$R_1(F)$[a]	0.0573
$wR_2(F^2)$[b]	0.1264
$\Delta\rho$(max/min) [e Å^{-3}]	2.163/–1.705

[a] $R_1 = [\Sigma||F_o| - |F_c||]/[\Sigma|F_c|]$. [b] $wR_2 = \{[\Sigma w(F_o^2 - F_c^2)^2]/[\Sigma w(F_o^2)^2]\}^{1/2}$ with $1/w = \sigma^2F_o^2 + (aP)^2 + bP$, $P = [F_o^2 + 2F_c^2]/3$, a = 0.0801, and b = 0.

Syntheses: All chemicals were commercially available and of reagent-grade quality and used as received. The cyclic precursor $(NMe_4)_xK_{2-x}[I_2Mo_{10}S_{10}O_{10}(OH)_{10}(H_2O)_5]\cdot 20H_2O$ was prepared as described previously.[43] The monovacant heteropolytungstate α_2-$K_{10}P_2W_{17}O_{61}\cdot 20H_2O$ was prepared according to the procedure described by Contant.[44]

$K_9Na_7[(P_2W_{17}O_{61})_2\{Mo_4S_4O_4(OH_2)_2\}]\cdot 50H_2O$ (1): $(NMe_4)_xK_{2-x}[I_2Mo_{10}S_{10}O_{10}(OH)_{10}(H_2O)_5]\cdot 20H_2O$ (2.8 g; 1.17 mmol) was hydrolyzed in 0.3 mol L^{-1} HCl (85 mL). Then $K_{10}[\alpha_2$-$P_2W_{17}O_{61}]\cdot 20H_2O$ (20.0 g, 4.07 mmol) was poured into the solution under vigorous stirring. The color of the solution quickly turned from yellow to deep red-brown. After 30 min, potassium chloride (7 g, 93.9 mmol) was added, provoking the precipitation of the brown potassium salt. After 1 h of slow stirring, the solid was collected by filtration, washed with ethanol and diethyl ether, and dried in air to give 18.8 g of a brown powder. The crude product (10 g) was dissolved in a 0.5 mol L^{-1} NaCl solution (100 mL) and allowed to stand to crystallize at room temperature. A week after, needle-shaped brown crystals were collected. Yield: ≈50%). ^{31}P NMR [D_2O/H_2O (1:1)]: δ = –7.53, –13.38 ppm (1:1 intensity ratio of peaks). FTIR: $\tilde{\nu}$ = 1081 (m), 1052 (w), 1019 (w), 938 (s), 840 (m), 760 (m), 526 (m), 466 (w) cm^{-1}. $K_9Na_7[(P_2W_{17}O_{61})_2\{Mo_4S_4O_4(OH_2)_2\}]\cdot 50H_2O$: calcd. K 3.40, Na 1.55, P 1.20, W 60.38, Mo 3.71, S 1.24; found K 3.44, Na 1.46, P 1.30, W 58.41, Mo 3.72, S 1.25.

Supporting Information (see footnote on the first page of this article): Representation of the crystallographic disorder within the central $[H_4Mo_4S_4O_6]$ cluster and Arrhenius plots are presented.

Acknowledgments

This work was supported by the Centre National de la Recherche Scientifique (CNRS) and the Ministère de l'Education Nationale de l'Enseignement Supérieur et de la Recherche (MENESR). Dr. Marie-Madeleine Rohmer and Dr. Marc Bénard from the University of Strasbourg are gratefully acknowledged for DFT calculations and we think especially of Marie-Madeleine Rohmer, who unfortunately passed away too early. Dr. Bineta Keita from the University of Paris-Sud, Orsay, is also acknowledged for the preliminary electrochemical and electrocatalytical studies.

[1] A. Proust, R. Thouvenot, P. Gouzerh, *Chem. Commun.* **2008**, 1837–1852.
[2] B. Keita, L. Nadjo, *J. Mol. Catal. A* **2007**, *262*, 190–215.
[3] S. Hikichi, M. Kaneko, Y. Miyoshi, N. Mizuno, K. Fujita, M. Akita, *Top. Catal.* **2009**, *52*, 845–851.
[4] R. Prudent, V. Moucadel, B. Laudet, C. Barette, L. Lafanechere, B. Hasenknopf, J. Li, S. Bareyt, E. Lacote, S. Thorimbert, M. Malacria, P. Gouzerh, C. Cochet, *Chem. Biol.* **2008**, *15*, 683–692.
[5] A. Ogata, H. Yanagie, E. Ishikawa, Y. Morishita, S. Mitsui, A. Yamashita, K. Hasumi, S. Takamoto, T. Yamase, M. Eriguchi, *Br. J. Cancer* **2008**, *98*, 399–409.
[6] A. Giusti, G. Charron, S. Mazerat, J. D. Compain, P. Mialane, A. Dolbecq, E. Rivière, W. Wernsdorfer, R. N. Biboum, B. Keita, L. Nadjo, A. Filoramo, J. P. Bourgoin, T. Mallah, *Angew. Chem.* **2009**, *121*, 5049; *Angew. Chem. Int. Ed.* **2009**, *48*, 4949–4952.
[7] J. D. Compain, P. Mialane, A. Dolbecq, I. M. Mbomekalle, J. Marrot, F. Sécheresse, E. Rivière, G. Rogez, W. Wernsdorfer, *Angew. Chem.* **2009**, *121*, 3123; *Angew. Chem. Int. Ed.* **2009**, *48*, 3077–3081.
[8] P. Kogerler, B. Tsukerblat, A. Müller, *Dalton Trans.* **2010**, *39*, 21–36.
[9] U. Kortz, A. Müller, J. van Slageren, J. Schnack, N. S. Dalal, M. Dressel, *Coord. Chem. Rev.* **2009**, *253*, 2315–2327.
[10] L. M. R. Albelo, A. R. Ruiz-Salvador, D. W. Lewis, A. Gomez, P. Mialane, J. Marrot, A. Dolbecq, A. Sampieri, C. Mellot-Draznieks, *Phys. Chem. Chem. Phys.* **2010**, *12*, 8632–8639.
[11] J. Thiel, C. Ritchie, H. N. Miras, C. Streb, S. G. Mitchell, T. Boyd, M. N. C. Ochoa, M. H. Rosnes, J. McIvet, D. L. Long, L. Cronin, *Angew. Chem. Int. Ed.* **2010**, *49*, 6984–6988.
[12] D. L. Long, R. Tsunashima, L. Cronin, *Angew. Chem.* **2010**, *122*, 1780; *Angew. Chem. Int. Ed.* **2010**, *49*, 1736–1758.
[13] T. G. Spiro (Ed.), *Molybdenum Enzymes*, Wiley, New York, **1985**.
[14] E. I. Stiefel, D. Coucouvanis, W. E. Newton (Eds.), *Molybdenum Enzymes, Cofactors and Model Systems*, ACS Symposium Series 535, American Chemical Society, Washington, DC, **1993**.
[15] R. R. Eady, *Chem. Rev.* **1996**, *96*, 3013–3030.
[16] D. Coucouvanis, *Adv. Inorg. Chem.* **1998**, *45*, 1–73.
[17] A. M. Appel, D. L. DuBois, M. Rakowski-DuBois, *J. Am. Chem. Soc.* **2005**, *127*, 12717–12726.
[18] L. L. Lopez, P. Bernatis, J. Birnbaum, R. C. Haltiwanger, M. Rakowski-DuBois, *Organometallics* **1992**, *11*, 2424–2435.
[19] J. C. V. Laurie, L. Duncan, R. C. Haltiwanger, R. T. Weberg, M. Rakowski-DuBois, *J. Am. Chem. Soc.* **1986**, *108*, 6234–6241.
[20] S. Duval, S. Floquet, C. Simonnet-Jégat, J. Marrot, R. N. Biboum, B. Keita, L. Nadjo, M. Haouas, F. Taulelle, E. Cadot, *J. Am. Chem. Soc.* **2010**, *132*, 2069–2077.
[21] B. Keita, S. Floquet, J. F. Lemonnier, E. Cadot, A. Kachmar, M. Bénard, M. M. Rohmer, L. Nadjo, *J. Phys. Chem. C* **2008**, *112*, 1109–1114.
[22] T. Shibahara, *Coord. Chem. Rev.* **1993**, *123*, 73–147.
[23] M.-A. Pilette, J. Marrot, F. Sécheresse, E. Cadot, *Inorg. Chim. Acta* **2010**, *363*, 4253–4261.
[24] J. Marrot, M. A. Pilette, F. Sécheresse, E. Cadot, *Inorg. Chem.* **2003**, *42*, 3609–3615.
[25] E. Cadot, M. A. Pilette, M. Marrot, F. Sécheresse, *Angew. Chem.* **2003**, *115*, 2223; *Angew. Chem. Int. Ed.* **2003**, *42*, 2173–2176.
[26] V. Béreau, E. Cadot, H. Bogge, A. Müller, F. Sécheresse, *Inorg. Chem.* **1999**, *38*, 5803–5808.
[27] E. Cadot, V. Béreau, B. Marg, S. Halut, F. Sécheresse, *Inorg. Chem.* **1996**, *35*, 3099–3106.
[28] S. C. Termes, M. T. Pope, *Transit. Met. Chem.* **1978**, *3*, 103–108.
[29] W. T. Randall, T. J. R. Weakley, R. G. Finke, *Inorg. Chem.* **1993**, *32*, 1068–1071.
[30] A. Müller, V. P. Fedin, C. Kuhlmann, H. D. Fenske, G. Baum, H. Bogge, B. Hauptfleisch, *Chem. Commun.* **1999**, 1189–1190.
[31] I. D. Brown, D. Alternatt, *Acta Crystallogr., Sect. B* **1985**, *41*, 244–247.
[32] N. E. Brese, M. O'Keefe, *Acta Crystallogr., Sect. B* **1991**, *47*, 192–197.
[33] D. Coucouvanis, A. Hadjikyriacou, A. Toupadakis, S.-M. Koo, O. Ileperuma, M. Draganjac, A. Salifoglou, *Inorg. Chem.* **1991**, *30*, 754–767.
[34] G. Bunzey, J. H. Enemark, J. K. Howie, D. T. Sawyer, *J. Am. Chem. Soc.* **1977**, *99*, 4168–4170.
[35] T. Chandler, D. L. Lichtenberger, J. H. Enemark, *Inorg. Chem.* **1981**, *20*, 75–77.
[36] A. Hadjikyriacou, D. Coucouvanis, *Inorg. Chem.* **1989**, *28*, 2169–2177.
[37] V. S. Korenev, A. G. Boulay, A. Dolbecq, M. N. Sokolov, A. Hijazi, S. Floquet, V. P. Fedin, E. Cadot, *Inorg. Chem.* **2010**, *49*, 9740–9742.
[38] T. M. Anderson, C. L. Hill, *Inorg. Chem.* **2002**, *41*, 4252–4258.
[39] G. M. Sheldrick, *SADABS; program for scaling and correction of area detector data*, University of Göttingen, Göttingen, **1997**.
[40] R. H. Blessing, *Acta Crystallogr., Sect. A* **1995**, *51*, 33–38.
[41] G. M. Sheldrick, *Acta Crystallogr., Sect. A* **1990**, *46*, 467–473.
[42] G. M. Sheldrick, *SHELX-TL version 5.03, Software Package for the Crystal Structure Determination*, Siemens Analytical X-ray Instrument Division, Madison, WI, **1994**.
[43] E. Cadot, B. Salignac, J. Marrot, A. Dolbecq, F. Sécheresse, *Chem. Commun.* **2000**, 261–262.
[44] R. Contant, *Inorg. Synth.* **1990**, *27*, 107.

Received: March 2, 2011
Published Online: July 11, 2011

